JACS
JOURNAL OF THE AMERICAN CHEMICAL SOCIETY

ARTICLE

pubs.acs.org/JACS

Super Flexibility of a 2D Cu-Based Porous Coordination Framework on Gas Adsorption in Comparison with a 3D Framework of Identical Composition: Framework Dimensionality-Dependent Gas Adsorptivities

Atsushi Kondo,[*,†,□] Hiroshi Kajiro,[*,‡] Hiroshi Noguchi,[§] Lucia Carlucci,[∥] Davide M. Proserpio,[∥] Gianfranco Ciani,[∥] Kenichi Kato,[⊥] Masaki Takata,[⊥] Hiroko Seki,[#] Masami Sakamoto,[▽] Yoshiyuki Hattori,[○] Fujio Okino,[○] Kazuyuki Maeda,[¶] Tomonori Ohba,[§] Katsumi Kaneko,[+] and Hirofumi Kanoh[*,§]

[†]Collaborative Innovation Center for Nanotech FIBER (nanoFIC), Shinshu University, 3-15-1 Tokida, Ueda 386-8567, Japan

[‡]Nippon Steel Corporation, Shintomi, Futtsu, Chiba 293-8511, Japan

[§]Graduate School of Science, Chiba University, 1-33, Yayoi-cho, Inage-ku, Chiba 263-8522, Japan

[∥]Università degli Studi di Milano, Dipartimento di Chimica Strutturale e Stereochimica Inorganica, Via G. Venezian 21, 20133 Milano, Italy

[⊥]RIKEN SPring-8 Center, 1-1-1 Kouto, Sayo-cho, Sayo-gun, Hyogo 679-5148, Japan

[#]Chemical Analysis Center, Chiba University, 1-33 Yayoi, Inage, Chiba, 263-8522 Japan

[▽]Department of Applied Chemistry and Biotechnology, Graduate School of Engineering, Chiba University, 1-33, Yayoi-cho, Inage-ku, Chiba 263-8522, Japan

[○]Department of Chemistry, Faculty of Textile Science and Technology, Shinshu University, 3-15-1 Tokida, Ueda, 386-8567, Japan

[¶]Department of Applied Chemistry, Tokyo University of Agriculture and Technology, 2-24-16 Koganei, Naka-cho 184-8588, Japan

[+]Research Center for Exotic Nanocarbons, Shinshu University, 4-17-1 Wakasato, Nagano-city 380-8553, Japan

Supporting Information

ABSTRACT: Selective synthetic routes to coordination polymers $[Cu(bpy)_2(OTf)_2]_n$ (bpy = 4,4′-bipyridine, OTf = trifluoromethanesulfonate) with 2- and 3-dimensionalities of the frameworks were established by properly choosing each different solvent−solution system. They show a quite similar local coordination environment around the Cu(II) centers, but these assemble in a different way leading to the 2D and 3D building-up structures. Although the two kinds of porous coordination polymers (PCPs) both have flexible frameworks, the 2D shows more marked flexibility than the 3D, giving rise to different flexibility-associated gas adsorption behaviors. All adsorption isotherms for N_2, CO_2, and Ar on the 3D PCP are of type I, whereas the 2D PCP has stepwise gas adsorption isotherms, also for CH_4 and water, in addition to these gases. The 3D structure, having hydrophilic and hydrophobic pores, shows the size-selective and quadrupole-surface electrical field interaction dependent adsorption. Remarkably, the 2D structure can accommodate greater amounts of gas molecules than that corresponding to the inherent crystallographic void volume through framework structural changes. In alcohol adsorption isotherms, however, the 2D PCP changes its framework structure through the guest accommodation, leading to no stepwise adsorption isotherms. The structural diversity of the 2D PCP stems from the breathing phenomenon and expansion/shrinkage modulation.

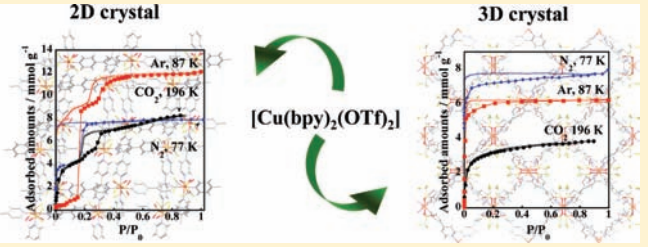

1. INTRODUCTION

In coordination chemistry, porous coordination polymers (PCPs) or metal−organic frameworks (MOFs) have gained much attention in a few decades not only because of their intriguing variety of architectures and topologies[1−9] but also for potential application functionalities of gas storage,[10−16] separation,[17−22] catalysis,[23−28] sensor,[29] magnetism,[30−34] nonlinear optics,[35−38] and ion exchange.[39]

Since one of the most important properties of PCPs is the framework flexibility, because it has the potential to improve their unique functionalities, many PCPs exhibiting a wide range of flexible behavior have been reported.[40−59] The specific functions of such materials highly depend on the structural characteristics,

Received: February 16, 2011
Published: June 14, 2011

Scheme 1. Example of the Relationship between Framework Dimensionality and Softness/Rigidness of the Structure

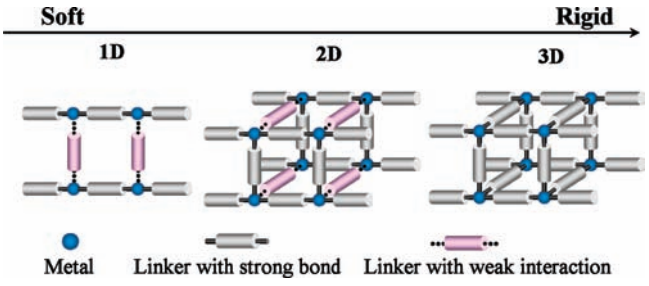

and the framework dimensionality is one of the most effective factors. For example, if weak interactions among 1D chains are replaced by strong bonds through rigid linkers, the resultant framework is a 2D network with lower flexibility; furthermore, if 2D sheets with weak interactions mutually connect via strong bondings, a more rigid 3D network is obtained (Scheme 1).[60,61] As a result, single frameworks with higher dimensionality may have less possibility to show high flexibility. Nevertheless, the effect of the structural dimensionality on the flexibility is not so clear because many factors can contribute to the flexible behavior, such as the strength of bonds or interactions through linkers and their coordination modes toward the metal centers.

Previously, we showed a unique adsorption property, i.e., "gate adsorption", of a variety of gases on an elastic layer-structured MOF (ELM), $[Cu(bpy)_2(BF_4)_2]_n$ (ELM-11) (bpy = 4,4′-bipyridine),[62−64] and we indicated that the expansion/shrinkage modulation of the ELM is the reason for the gate adsorption.[65] The unique gas adsorption phenomenon of the ELM occurs through a new chlatrate lattice formation between the ELM and the guest gas molecules.[66] We also showed a stepwise N_2 adsorption on an analogous ELM, $[Cu(bpy)_2(OTf)_2]_n$ (ELM-12) (OTf = trifluoromethanesulfonate), stemming from micropore filling and a subsequent gate adsorption.[67] MIL-53 (Cr) also shows similar adsorption behaviors coming from pore-shape distortion, and the responsive transformation depends on the nature of adsorbates.[68,69] The adsorptivities of various kinds of gases on ELM-12 are not yet clear and need to be investigated for a better understanding of the responsive adsorption and for its application to highly efficient storage and separation of gases such as CO_2 and CH_4.

We established simple routes to control the dimensionality of different PCPs with exactly the same framework composition, $[Cu(bpy)_2(OTf)_2]_n$, by choosing appropriate solvent−solution systems which consist of $Cu(OTf)_2$/water and bpy/ethanol with different kinds of alcoholic solvents for an intermediate layer. Though the Cu(II) nodes have quite similar local coordination structures, they are connected in different ways to form the 2D and 3D frameworks. The term "supramolecular network isomers"[4] was used to describe a pair of PCPs like these, and what is more interesting, they can be considered ideal model systems to elucidate the relationship between framework flexibility and dimensionality of PCPs.

As the structural flexibility of PCPs can be sensitively detected by gas adsorption, adsorption studies of molecules with different properties on 2D and 3D PCPs are strongly requested. In this article, we present the syntheses, structures, gas adsorption properties of N_2 (77 K), CO_2 (196 and 273 K), Ar (87 K), and H_2 (77 K) on the 2D and 3D PCPs, and vapor adsorption of water and some kinds of alcohols (303 K), as well as high-pressure adsorption of H_2 (77 and 303 K), CH_4 (258 K), and CO_2 (273 K) on the 2D PCP. The effect of the structural dimensionality of the PCPs on the structural flexibilities is discussed with relevance to the molecular adsorptivities.

2. EXPERIMENTAL SECTION

Selective Synthesis of Crystalline PCPs with Different Dimensionality. The 2D and 3D PCPs are synthesized by a basically similar procedure. A pure alcohol was carefully added onto an aqueous solution of $Cu(OTf)_2$, and then an ethanolic solution of bpy was carefully layered over this solution. When the interlayer phase of the pure alcohol is methanol, ethanol, 1-propanol, and 1-buthanol, blue crystals of the 2D PCPs were obtained (named **1**[67] for methanol, **2**[67] for ethanol, **3** for 1-propanol, and **4** for 1-buthanol, respectively). Compounds **1**−**4** are isostructural with slightly different interlayer distances and different unit cell volumes. On the other hand, blue crystals of the 3D PCPs were obtained when using 1-hexanol and 1-octanol as the interlayer phase (named **5** for 1-hexanol and **6** for 1-octanol). In addition, we can also obtain crystals of the 3D PCP **7** with a water−DMSO system.

It is worth noting that we have observed that crystals of **4** left to stand in the mother liquor for very long times (about one year) convert to 3D PCP, as confirmed by single-crystal X-ray diffraction. Similar long time spending experiments carried out with crystals of **1**, **2**, and **3** did not show appreciable 2D to 3D transformation.

The detailed synthetic procedures are as mentioned below.

Synthesis of Crystals of ***1***−***6***. A pure alcohol (1.0 mL) was carefully added (30.0 mL/h) onto an aqueous $Cu(OTf)_2$ solution (30 mM, 10.0 mL) in a straight glass vial, and then a solution of bpy/ethanol solution (60.0 mM, 10.0 mL) was layered onto the alcohol layer (30.0 mL/h), at room temperature. The glass vial was capped and left to stand. After a few weeks, plate (**1**−**4**) and block (**5** and **6**) shaped dark blue crystals were obtained, which were collected by filtration and washed with small amounts of distilled water and alcohol.

Synthesis of Crystals of ***7***. Distilled water (10.0 mL) was carefully added (30.0 mL/h) to a solution of bpy/DMSO (80.0 mM, 62.5 mL) in a square-shaped glass vial, and then an aqueous $Cu(OTf)_2$ solution (160 mM, 15.7 mL) was layered onto the water layer (30.0 mL/h) at room temperature. The glass vial was capped and left for seven days, and then the cap was opened. After a few weeks the block-shaped crystals were grown. The crystals were filtered off, washed with distilled water, and dried in air. These crystals gradually lose their transparency in air, and therefore the single-crystal X-ray diffraction measurements were carried out at low temperature by using the crystals from the mother liquid directly.

X-ray Single-Crystal Structural Determinations. Data were collected on a Bruker SMART CCD area detector diffractometer (Mo Kα radiation λ = 0.71073 Å) at 150 K for **3** by the ω scan method. Data were collected on a Bruker APEX II CCD area detector diffractometer (Mo Kα radiation λ = 0.71073 Å) at 173 K for **4**, **5**, and **6** and at 183 K for **7** by the ω scan method. Empirical absorption corrections (SADABS) were applied in all cases. The structures were solved by direct methods (SIR97) and refined by full matrix least-squares on F^2 (SHELX97). Anisotropic thermal factors were assigned to all non-hydrogen atoms with full occupancy. During the refinements of all structures, several residual peaks were found corresponding to highly disordered guest molecules. Their contribution was subtracted from the observed structure factors according to the BYPASS procedure[70] that was implemented in PLATON with the command SQUEEZE. The crystallographic parameters are summarized in Table 1 and ref 71.

Thermal Gravimetric (TG), In Situ X-ray Powder Diffraction (XRPD), and In Situ IR Measurements. TG analyses were

Table 1. Single-Crystal X-ray Data for 1−7[a]

compound	1	2	3	4	5	6	7
intermediate solvent	methanol	ethanol	1-propanol	1-butanol	1-hexanol	1-octanol	water
formula	$C_{22}H_{16}CuF_6N_4O_6S_2$	$C_{26}H_{30}CuF_6N_4O_9S_2$	$C_{25}H_{24}CuF_6N_4O_7S_2$	$C_{22}H_{16}CuF_6N_4O_6S_2$	$C_{22}H_{16}CuF_6N_4O_6S_2$	$C_{22}H_{16}CuF_6N_4O_6S_2$	$C_{22}H_{16}CuF_6N_4O_6S_2$
fw	674.05	784.20	736.14	674.05	674.05	674.05	674.05
lattice	orthorhombic	orthorhombic	orthorhombic	orthorhombic	tetragonal	tetragonal	tetragonal
a, Å	16.158(3)	16.743(9)	16.497(3)	16.510(3)	28.5955(13)	28.564(2)	28.546(4)
b, Å	13.688(3)	14.532(8)	14.296(3)	14.417(3)	28.5955(13)	28.564(2)	28.546(4)
c, Å	15.319(3)	14.723(8)	14.869(3)	14.910(3)	18.0782(8)	18.2725(13)	18.064(4)
V, Å^3	3388.3(12)	3538(3)	3506.7(12)	3548.9(12)	14782.6(12)	14908.6(18)	14720(4)
space group	*Pbna* (no. 60)	$Pn2_1a$ (no. 33)	*Pnna* (no. 52)	*Pnna* (no. 52)	$I4_1/acd$ (no. 142)	$I4_1/acd$ (no. 142)	$I4_1/acd$ (no. 142)
Z	4	4	4	4	16	16	16
T, K	150	150	150	173	173	173	183

[a] Crystal structures for compounds **1** and **2** were reported elsewhere.[65] The nonstandard setting $a\bar{c}b$ is used for **1** and **2** for comparison with **3** and **4**. Crystallographic details for **3**−**7** are reported in ref 71.

performed on a Seiko Instruments Inc. EXSTAR 6000 system under N_2 gas flow (200 mL/min). The TG measurements were carried out from room temperature to 773 K at a heating rate of 3 K/min. The in situ X-ray powder diffraction (XRPD) measurements were performed on an improved Bruker MXP3 system with graphite-monochromated Cu Kα radiation (λ = 1.5406 Å) by a fixed time method operating at 1000 W power (40 kV, 25 mA). The synchrotron XRPD patterns were collected at BL02B2 SPring-8 with a large Debye−Scherrer camera.[72] The wavelength of the incident X-ray was λ = 1.0005 ± 0.0005 Å. The temperature was controlled in a wide range by a low-temperature nitrogen gas blower. In situ IR spectra of the 3D PCP were recorded by the FT-IR spectrometer (JASCO FT/IR-550, JASCO) with temperature- and pressure-controlling systems.

Gas Adsorption Measurements. The adsorption isotherm measurements were carried out by a laboratory designed gravimetric apparatus (N_2 at 77 K, methanol, ethanol, 1-propanol, and water at 303 K) and an automatic volumetric apparatus (autosorb-1, Quantachrome, CO_2 at 196 and 273 K, Ar at 87.3 K, and H_2 at 77 K). The high-pressure adsorption isotherms were measured by a gravimetric system (Cahn1100 balance, H_2 at 77 and 303 K, CH_4 at 258 K, and CO_2 at 273 K). Because the XRD patterns of guest-free compounds of **1**−**4** are almost the same, **2** was used for gas adsorption experiments as a representative of the 2D PCP. Compound **7** was selected as a representative of the 3D PCP for the same reason. The powder samples were pretreated under vacuum ($<10^{-2}$ Pa) at 363 K for the 2D PCP and at 383 K for the 3D PCP for 2 h before each gas adsorption measurement.

3. RESULTS AND DISCUSSIONS

Crystal Structures of the 2D and 3D PCPs. The single-crystal X-ray diffraction analyses reveal that the Cu(II) ions in all the seven compounds are surrounded by four bpy ligands in equatorial position and two OTf anions in axial position forming a slightly distorted octahedral coordination geometry (Figure 1a). The structures of **1**−**4** have 2D square-grid (SG, 4^4 or **sql**) sheets (Cu···Cu in the range 11.11−11.15 Å, Figure 1b) comprising Cu(II) ions and bridging bpy ligands that are stacking each other in an *ABAB* fashion (Figure 1c, 1d, and Figure 1S, Supporting Information). Notwithstanding the same topological motif, crystals of **1**−**4** show different interlayer distances (Table 2). The neighboring 2D sheets in **2** are connected by hydrogen bondings via two guest ethanol molecules and one water molecule per molecular formula with a relatively long interlayer distance (7.17 Å) (Figure 2S and Table 1S, Supporting Information). On the other hand, defined guest molecules are not observed in **1**, and a weak interlayer interaction is present between oxygen atoms of OTf anions and hydrogen atoms of bpy ligands.[67] The interlayer distance (6.84 Å) of **1** is the smallest in the four crystals (**1**−**4**), while those of **3** and **4** (7.15 and 7.21 Å, respectively) are comparable to or slightly longer than that of **2**. In addition to the different interlayer distances, the 2D SG also shows the structural change associated to the previously called "breathing" transformation.[47] In compounds **2**−**4**, the square windows are rather distorted toward a rhombic-meshed geometry, while in **1** a more regular geometry is evidenced. The same distortion of the square layers is also present in the guest-free 2D species. Because the structure of **1** can be thought of as the intermediate state between the guest-containing states such as **2**−**4** and the guest-free state, the guest removal should occur through at first (i) the relaxation of the distortion and (ii) the following redistortion of the 2D SG (Figure 2). The crystals of **2** left in the air for over several days recover the original structure by immersion into the mother liquid, indicating reversible structural transformation induced by guest molecules. Interestingly, the structural change implies a process different from what was observed for the material MIL-53(Cr) which is well-known for the breathing effect. The flexibility in another dimension should influence the unique structural change process. The expansion/shrinkage modulation and the breathing transformation occur in a concerted fashion and affect the unit cell volumes and the void volumes. Comparing them with those of the guest-free state, the standardized unit cell volume (Z = 4) and the void volume change by 327−488 Å^3 (10.6−15.9% of the unit cell volume) and 0.048−0.11 mL/g (34−75% of the void volume), respectively.[73] The void volume of the guest-free 2D PCP is 0.14 mL/g. These results show that the 2D SG stacking compounds can have various structures accompanied by the accommodation of guest molecules.

The structure of the 3D PCP in **5**−**7** is similar to that reported before (2-fold interpenetrated 4^28^4-**lvt** topology).[74] There are two kinds of channels (hydrophilic and hydrophobic) due to the unique binding system irrespective of the similar coordination geometry around the Cu(II) ion and the same building units

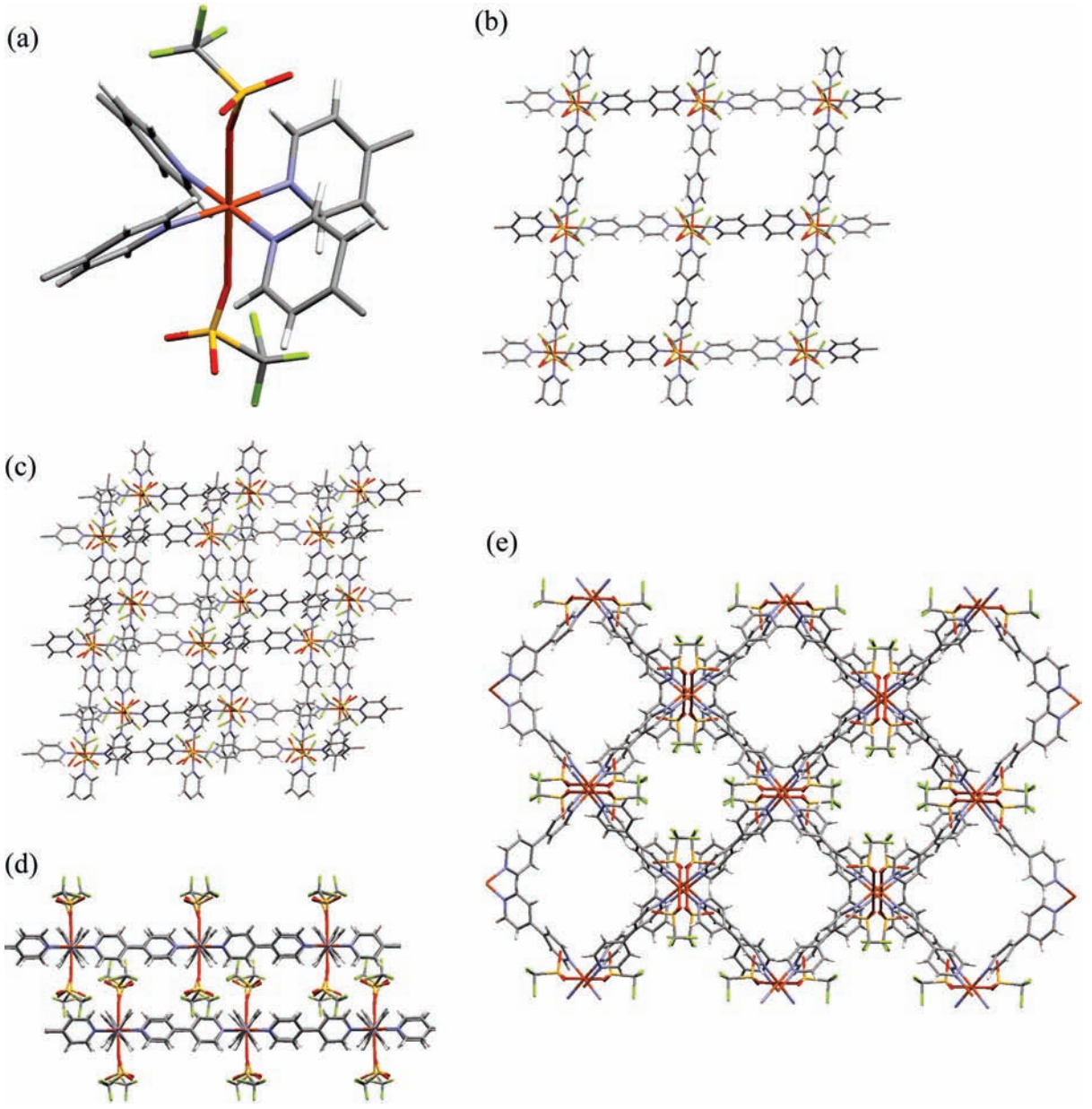

Figure 1. Local coordination structure of the Cu(II) ion in 2D and 3D PCPs (a). The 2D SG sheet in 2D PCP (b), top view (c), and side view (d) of stacking structure of the square grid sheets. The view of 3D PCP with hydrophilic and hydrophobic pores along the *c* axis (e).

Table 2. Interlayer Distance, Standardized Unit Cell Volume ($Z = 4$), and Calculated Void Volume of 2D Crystals 1−4[a]

crystal	1	2	3	4	guest-free
interlayer distance, Å	6.84	7.17	7.15	7.21	6.30
unit cell volume, Å^3	3388	3538	3507	3549	3061
void volume, Å^3 × 10^3	0.848	1.10	–	1.02	0.627
mL/g	0.189	0.245	–	0.227	0.14
(%)	(25.0%)	(31.0%)	–	(28.7%)	(20.5%)

[a] The unit cell volume of the guest-free PCP is standardized to correspond to other crystals.

present in the 2D PCP (Figure 1e and Figure 3S, Supporting Information). The two kinds of channels that align along the *c* axis alternate as a chessboard. The hydrophilic one is constructed by the stacking of bent squares, whereas the hydrophobic one is formed by double 4_1 helical chains entangled along the *c* axis. The size of the hydrophilic channel is smaller than that of the hydrophobic one because of the presence of OTf anions in the former ones. Therefore, the hydrophobic accessible volume is

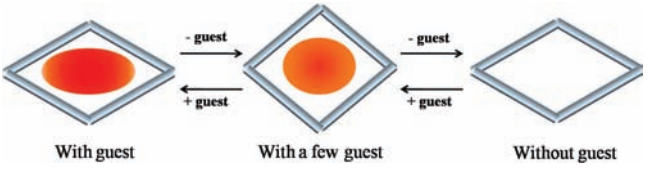

Figure 2. Schematic representation of 2D SG transformation through the guest removal.

Table 3. Calculated Hydrophilic and Hydrophobic Pore Volume of 3D PCPs 5−7[a]

crystal	5	6	7	average
hydrophilic pore volume, $Å^3 \times 10^3$	0.492	0.465	0.429	0.462
mL/g	0.110	0.104	0.0957	0.103
(%)	(13.3%)	(12.5%)	(11.6%)	(12.5%)
hydrophobic pore volume, $Å^3 \times 10^3$	0.828	0.905	0.841	0.858
mL/g	0.185	0.203	0.188	0.192
(%)	(22.4%)	(24.4%)	(22.9%)	(23.2%)
total void volume, $Å^3 \times 10^3$	1.32	1.37	1.27	1.32
mL/g	0.295	0.307	0.284	0.295
(%)	(35.7%)	(36.9%)	(34.5%)	(35.7%)

[a] These values are standardized in $Z = 4$ to compare the values of 2D PCPs.

larger than that of the hydrophilic one in **5**−**7** (Table 3). Comparing the unit cell parameters and pore parameters, slight deviations can be seen, showing the flexibility of the 3D framework. The average pore volume of the 3D PCPs **5**−**7** is 0.295 mL/g [hydrophilic pore, 0.103 mL/g (12.5%); hydrophobic pore, 0.192 mL/g (23.2%), respectively].[73] The 3D PCP has the higher porosity, compared to the guest-free 2D PCP (Tables 2 and 3).

An important structural difference in the two types of PCPs consists of the fact that in the 2D species all the inside guest-accessible voids are hydrophilic regions (i.e., the interlayer spaces) while the 3D networks exhibit (smaller) hydrophilic channels and (larger) hydrophobic ones. This can explain the selective syntheses of compounds **1**−**6**; that is, with the growing length of the chains of the *n*-alcohols used, implying an increased hydrophobic contribution, the 3D architectures seem favored. The borderline compound **4** (*n*-buthanol) has been observed to give both "supramolecular isomeric" frameworks.

Adsorption of N_2, CO_2, and Ar on 3D PCP. Figure 3a shows the adsorption isotherms of N_2 (77K), CO_2 (196 K), and Ar (87 K) on the 3D PCP. All of the isotherms show a steep uptake at the low relative pressure region followed by the plateau region that can be categorized as type I of IUPAC classification. The shape of adsorption isotherms indicates the presence of uniform micropores with a deep potential well. In the isotherms of N_2 and Ar, a clear disagreement in adsorption and desorption branch is observed. This should come from a diffusion restriction due to the narrow pores at the low measuring temperature. On the other hand, a hysteresis loop in a low-pressure region is not observed for the CO_2 adsorption due to relatively higher measuring temperature. The maximum adsorption amounts at $P/P_0 = 1$ are highly dependent on the gas species. The adsorbed amount of N_2 is 2.1 times and that of Ar is 1.6 times larger than that of CO_2 in molar unit (N_2, 8.0 mmol/g, Ar, 6.2 mmol/g, CO_2, 3.8 mmol/g). Molecular adsorption in microporous systems has been described by the following Dubinin−Radushkevich (DR) equation:[75] $W/W_0 = \exp[-(A/E)^2]$, $A = RT \ln(P_0/P)$, $E = \beta E_0$.

Here W is the amount of adsorption at pressure P, W_0 the micropore volume, E_0 the characteristic adsorption energy, and β the affinity coefficient. βE_0 is associated with the isosteric heat of adsorption, $q_{st,\varphi=1/e}$, at the fractional filling φ of $1/e$ using the enthalpy of vaporization, ΔH_v, at the boiling point.

$$q_{st,\varphi=1/e} = \Delta H_v + \beta E_0$$

The obtained W_0 and $q_{st,\varphi=1/e}$ are summarized in Table 4. The W_0 value of N_2 is almost equivalent to the crystallographic total void volume of the 3D PCP, indicating the pore filling of N_2 molecules in both hydrophilic and hydrophobic pores. In contrast, the W_0 values of CO_2 and Ar seem to be comparable to the void volumes of hydrophilic and hydrophobic pores, respectively. If Ar molecules can be adsorbed in both pores, the estimated adsorbed amount of Ar from the micropore volume of N_2 (0.27 mL/g) and liquid density of Ar at boiling point (1.393 g/mL) is about 9.5 mmol/g, that is, quite larger than the experimental result (6.2 mmol/g). In the 3D PCP, the hydrophilic pore size is comparable to the size of adsorptives and smaller than the hydrophobic one. In addition, the molecular size of Ar (3.40 Å)[76] is larger than the one of N_2 (3.32 Å)[77] in

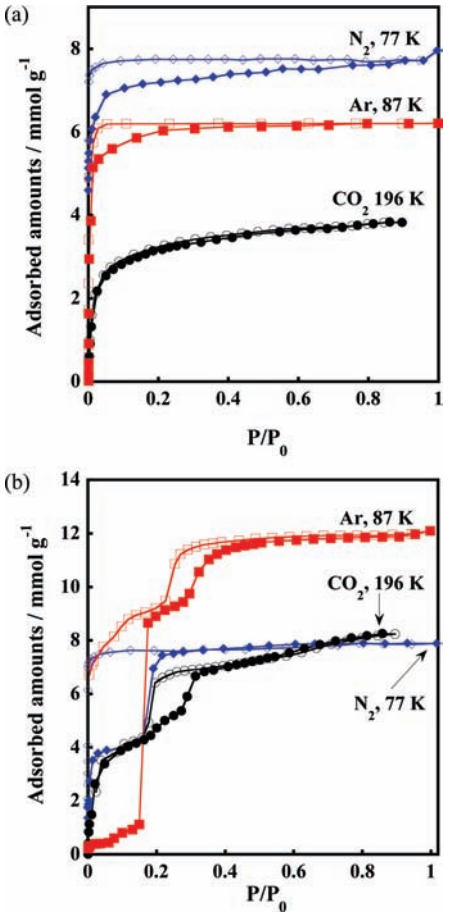

Figure 3. Adsorption isotherms of N_2 (77K), CO_2 (196 and 273 K), and Ar (87.3 K) on (a) 3D and (b) 2D PCPs. Solid and open symbols represent adsorption and desorption branches, respectively.

Table 4. Micropore Parameters of 3D PCP

	N_2	CO_2	Ar
W_0, mL/g	0.27[a]	0.095	0.19[a]
q_{st}, kJ/mol	20[a]	34	15[a]

[a] The estimations of micropore parameters were performed by using the desorption branches.

Table 5. Characteristic Parameters of Multisteps in the N_2 Adsorption Isotherm of 2D PCP from DR Plots

	adsorption			desorption	
	first	second	third	first	second
pressure, P/P_0	$<3 \times 10^{-3}$	$1 \times 10^{-2} < P/P_0 < 0.16$	$0.22 <$	$<2 \times 10^{-4}$	$>1 \times 10^{-2}$
W_0, mL/g	0.072	0.15	0.27	–	0.27
q_{st}, kJ/mol	20	11	9.9	10	16

minimum dimension. Therefore, it is reasonable to consider that Ar molecules cannot be adsorbed in the hydrophilic pores, that is, selective adsorption in the hydrophobic pores. Although the 3D PCP is relatively rigid compared with the 2D PCP, flexibility and slightly different structures of 3D PCP, corresponding to different guest molecules, have been detected. The details are not clear, but framework flexibility induced by guest−host interaction should influence the gas adsorptivities. In the case of adsorption of CO_2, that has a large quadrupole moment, the presence of polar groups on the surface is a requisite for sufficient adsorption with the aid of the quadrupole−surface field interaction even at the sublimation temperature.[78] Therefore, CO_2 molecules should be selectively adsorbed in the hydrophilic pores of smaller size. In situ IR spectroscopic examination at 196 K supports this behavior. The peak at 1182 cm^{-1}, assigned to the asymmetric mode ν_{as} of SO_3,[79] slightly but gradually shifts to a lower frequency (1172 cm^{-1}) with an isosbestic point, whereas peaks related to bpy ligand are not changed during the CO_2 adsorption (Figure 4S, Supporting Information). The IR results indicate that CO_2 molecules interact with OTf anions in the hydrophilic pore. The obtained $q_{st,\varphi=1/e}$ value from the CO_2 isotherm is 34 kJ/mol which is much greater than the sublimation heat of CO_2 at 194.7 K (25.2 kJ/mol). If all of CO_2 molecules are adsorbed only in the hydrophilic pores, the adsorbed density calculated with the adsorbed amount and crystallographic void volume is 1.53 g/mL which is comparable to that of dry ice (1.56 g/mL) at 193 K.

Adsorption of N_2, CO_2, and Ar on 2D PCP. The adsorption isotherms of N_2 (77K), CO_2 (196 K), and Ar (87 K) on the 2D PCP are shown in Figure 3b. All isotherms differ from the type I isotherms on the 3D PCP, showing some steps in both adsorption/desorption branches with a wide range of hysteresis loop. In the N_2 isotherm, there are three steps in the adsorption branch and two steps in the desorption branch (Figure 5S, Supporting Information). The values of W_0 and $q_{st,\varphi=1/e}$ at each step are obtained from DR analysis (Table 5). The first step in the adsorption having the largest $q_{st,\varphi=1/e}$ value should be the specific adsorption near Cu(II) ions because of the deepest potential well near the metal ion, which is supported by the uptake in the lowest pressure range. The W_0 value of the second uptake is equivalent to the crystallographic void volume of the guest-free 2D PCP; the second step should correspond to the micropore filling of N_2 molecules in the inherent micropores. The third steep uptake at P/P_0 = 0.16 must mainly stem from the expansion of the interlayer distance to form accessible free space corresponding about to the double of the crystallographic void volume of the guest-free 2D PCP,[67] which is comparable to the total pore volume of the 3D PCP. The uptake of the 3D PCP mainly derives from the micropore filling, while the 2D PCP adsorbs N_2 molecules by micropore filling, inducing the structural transformation that increases the micropore volume. The $q_{st,\varphi=1/e}$ values from adsorption/desorption branches on the 2D PCP are quite different, indicating the presence of energetically different adsorption sites and/or the consumption of energy through the framework structural change.

Table 6. Filling Percentage of the Original Crystallographic Pore Volume [a]

	2D	3D
gas species	filling percentage, %	
N_2	190	87
CO_2	160	35
Ar	250	58

[a] These percentages were calculated using the following densities (N_2, 0.808 g/mL; CO_2, 1.565 g/mL; Ar, 1.393 g/mL).

Although adsorption isotherms of CO_2 at 196 K and of Ar at 87 K on the 2D PCP show some stepwise uptakes in adsorption/desorption branches with hysteresis loops, the adsorptivities in the low-pressure region are remarkably different from each other. The CO_2 adsorption isotherm indicates the steep uptake, whereas the Ar adsorption shows a small increment of adsorption amount in the low relative pressure region. This means that the micropore size of the 2D PCP is smaller than an Ar atom and larger than a CO_2 molecule. Only Ar is nonpolar and spherical, being different from both N_2 and CO_2, and the size of Ar is the largest of the three species in minimum dimension (Lennard-Jones parameters: Ar, 3.40 Å; N_2, 3.32 Å; CO_2, 3.03 Å).[76,77,80] The above adsorption data indicate that the slight difference in the molecular shape, size, and polarity can be recognized by the flexible 2D PCP. An abrupt uptake like gate adsorption appears at P/P_0 = 0.15 after the slight rise in the Ar adsorption. The BET surface area below the uptake is 38 m^2/g which is much smaller than that from the N_2 adsorption isotherm (740 m^2/g). In the higher-pressure region after the steep uptake, the BET surface area drastically increases up to 630 m^2/g, indicating the adsorption into the micropores produced thanks to the structural transformation. These results show one important fact; that is, the micropore filling is not necessary to induce the structural transformation. The Ar adsorption mechanism is different from that of N_2 because the structure transformation occurs without the micropore filling whereas N_2 adsorption needs it as mentioned above. It is noteworthy that the 2D PCP adsorbs a large amount of Ar and CO_2, more than twice that for the 3D PCP, through the dynamic structural change, though the 2D PCP has less than half of void volume of the 3D PCP in the guest-free state. The evaluated filling percentages, those calculated from each adsorption amount, liquid, or solid density of adsorbate, and the crystallographic void volumes, are shown in Table 6 for comparison of adsorption capacities of the 2D and 3D PCPs. All of the filling percentages of the 2D PCP exceed 100%, whereas

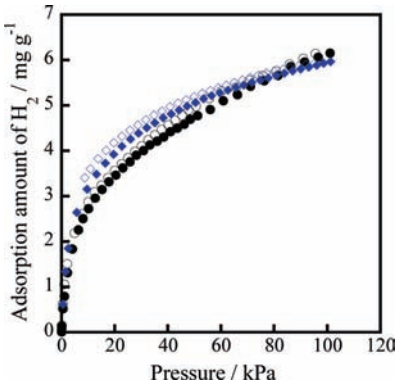

Figure 4. Hydrogen adsorption isotherms of 2D (rhombic) and 3D (circle) PCPs at 77 K. Solid and open symbols represent adsorption and desorption branches, respectively.

Table 7. Saturated H_2 Adsorption Amount W_L, The Quasi-Saturated Vapor Pressure P_{0q}, and Isosteric Heat of Adsorption at Fractional Filling of $1/e$, $q_{st,\varphi=1/e}$, on 2D and 3D PCPs

crystal	W_L, mg/g	P_{0q}, kPa	$q_{st,\varphi=1/e}$, kJ/mol
2D	7.1	700	3.8
3D	8.0	1030	3.4

the 3D PCP shows less than 100% of the filling percentage. Accordingly, the 2D PCP transforms its framework structure to accommodate a larger amount of guest molecules than the void volume of the original crystallographic structure, taking advantage of the flexible framework. On the other hand, the 3D PCP has less framework flexibility and adsorbs gas molecules only in the inherent pores of the more rigid lattice.

Supercritical H_2 Adsorption Properties of 2D and 3D PCPs. One of the most interesting features of the flexible PCPs is the adsorption properties of clean energy such as hydrogen and methane.[66,81−83] The H_2 adsorption isotherms at 77 K are shown in Figure 4. The shape of the isotherms on the 2D and 3D PCPs is of type I with no step, and a slight deviation in adsorption/desorption branches is observed. The 2D and 3D PCPs show the equivalent maximum adsorption amount at 101 kPa (2D PCP; 6.0 mg/g, 3D PCP; 6.2 mg/g). The isotherm on the 2D PCP shows a steeper uptake than that on the 3D PCP in the low-pressure region, being consistent with that of CO_2 adsorption at 273 K (Figure 6S, Supporting Information). Since both adsorption isotherms do not reach the saturation of adsorption, the saturated H_2 adsorption amount W_L is estimated from the Langmuir plot of the adsorption isotherms. Furthermore, the adsorption isotherms of supercritical H_2 are analyzed with the extended DR analysis to determine the quasi-saturated vapor pressure P_{0q} and $q_{st,\varphi=1/e}$ (Table 7).[84] Here, a smaller P_{0q} indicates a more quasi-vaporization of a supercritical gas due to the stronger molecule−pore interaction. If there is no structural change, the saturated H_2 adsorption amount on the 3D PCP should be larger than that of the 2D PCP assumed from the W_L values. On the other hand, the resultant P_{0q} and $q_{st,\varphi=1/e}$ values indicate the stronger adsorption affinity of a H_2 molecule to the 2D PCP than the 3D PCP. The adsorbed volumes of H_2 on the 2D and 3D PCP are estimated by using the liquid density of 0.077 mg/mL at the triple point to be 0.078 and 0.081 mL/g, respectively, corresponding to 55% and 27% filling of the crystallographic void volumes.

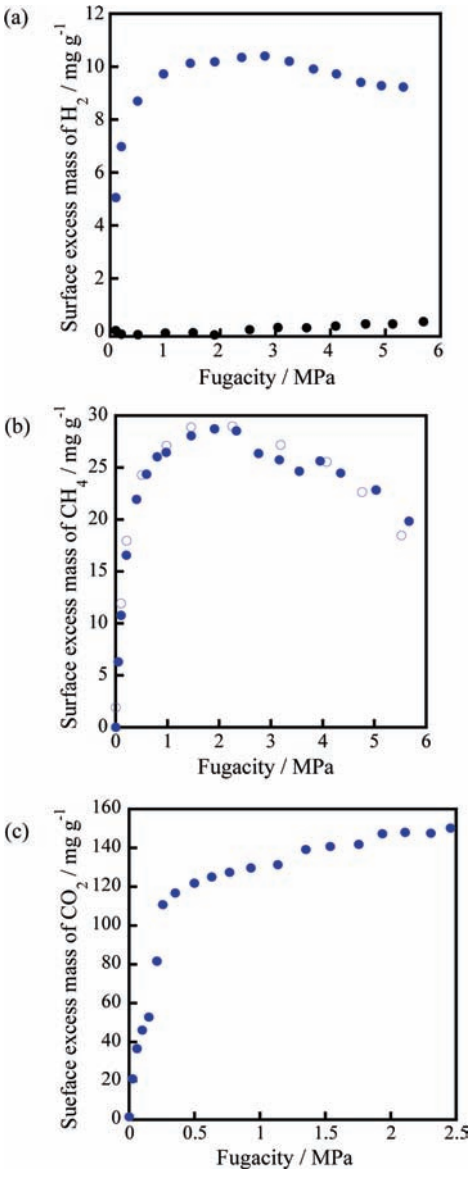

Figure 5. High-pressure adsorption isotherms of 2D PCP for H_2 at 77 K (blue) and 303 K (black) (a), CH_4 at 258 K (b), and CO_2 at 273 K (c). Solid and open symbols represent adsorption and desorption branches, respectively.

High-Pressure Gas Adsorptivities of the 2D PCP. For the understanding of gas adsorption properties of the 2D PCP in a wide pressure range, we performed the high-pressure H_2 adsorption measurements up to 6 MPa on the highly flexible 2D PCP at 77 and 303 K (Figure 5a). The surface excess amount of H_2 at 77 K increases up to 10.4 mg/g, which is larger than the saturated adsorption amount estimated by the Langmuir plot from the low-pressure adsorption isotherm, and no definite steps are observed. This result implies that structural changes can occur through a gas adsorption without definite adsorption jumps and/or folding points in an isotherm. The adsorption amount is almost nil up to 6 MPa at 303 K, indicating that the interaction between supercritical H_2 gas and the framework of the 2D PCP is too weak. That is, the stabilization energy gain due to the clathrate formation between H_2 and the 2D PCP should be smaller when compared with other gas species such as N_2, Ar, and CO_2.

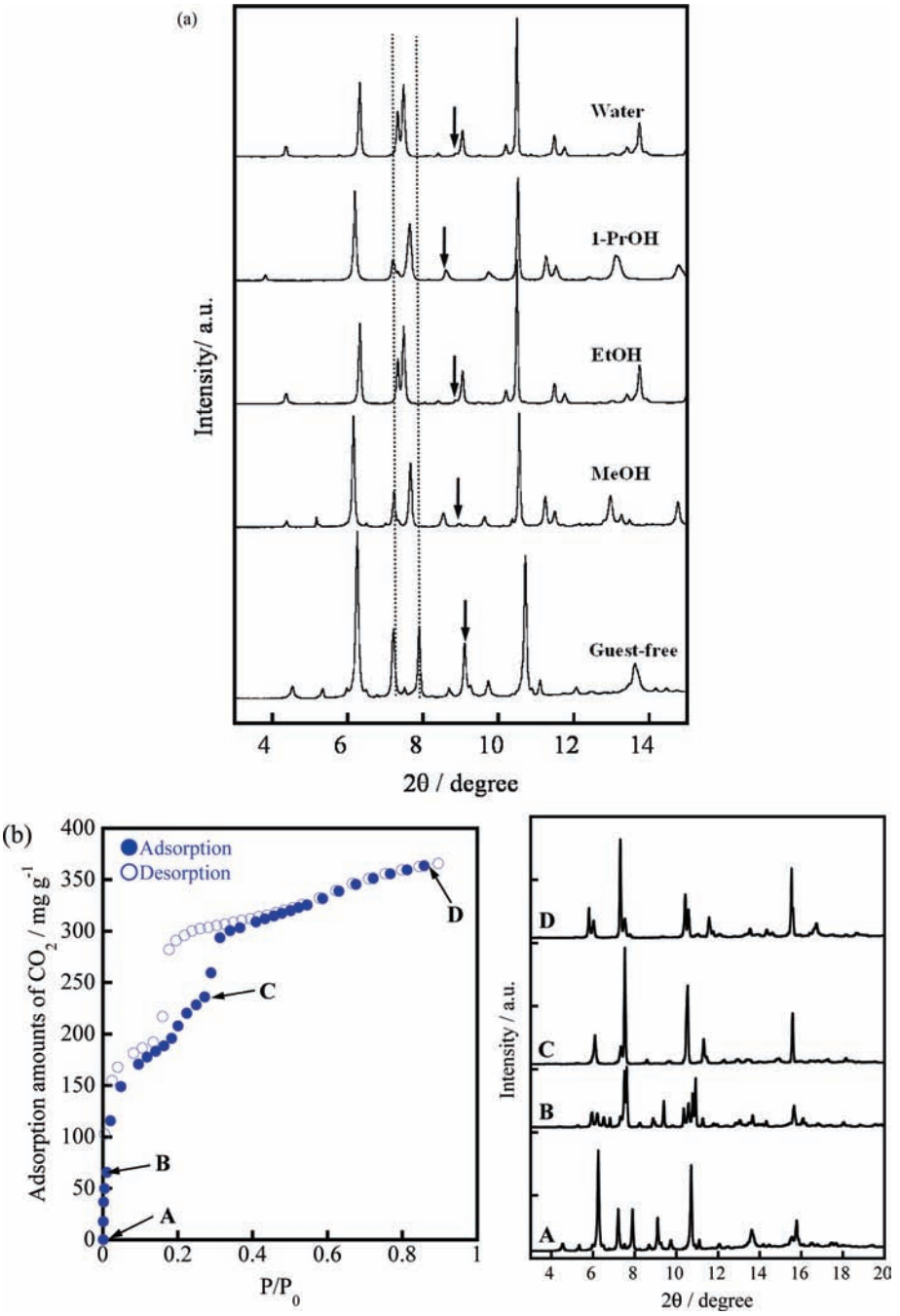

Figure 6. Synchrotron XRD patterns of (a) 2D PCP without guest, adsorbing methanol, ethanol, and 1-propanol at room temperature and (b) adsorbing CO_2 at 196 K at different pressures of points A, B, C, and D. Arrows show the diffraction peaks relating to the interlayer distances. Dotted lines indicate the diffraction peaks relating to the shape of 2D SG in the guest-free state. Those diffraction peaks of methanol, ethanol, 1-propanol, and water adsorbing 2D PCPs are between the two lines.

In recent years, CH_4 and CO_2, which have stronger interaction energy than H_2, have attracted much attention because they are the greenhouse gases, and furthermore, at the same time, CH_4 is regarded as one of the clean energies. Figure 5b shows the high-pressure CH_4 adsorption isotherm on the 2D PCP at 258 K. The packing density of the pores with molecules becomes difficult to be increased due to the presence of pore walls at a higher pressure, and thereby the surface excess mass slightly decreases with the increase of the pressure. The slight folding point that is observed at 4 MPa should come from the structural change of the framework. The high-pressure CO_2 adsorption isotherm at 273 K is shown in Figure 5c. A definite steep uptake at around 0.2 MPa is observed, although the adsorption jump is observed below 0.1 MPa at 196 K. If CO_2 molecules fill the inherent micropores of the guest-free 2D PCP at this point, the adsorbed CO_2 density is 0.38 g/mL, which is similar to that calculated from the volume at the first folding point (196 K, $P/P_0 = 10^{-4}$). These results indicate that the interaction between gas molecules and adsorbents plays an essential role to induce the dynamic structural changes to form the clathrate compound.

Structure-Expanding Guest Accommodation Ability of the 2D PCP. As shown above, the 2D PCP shows a variety of unique stepwise gas adsorption isotherms, suggesting an explicit structure expansion of the 2D SG sheets on accommodation of guest molecules. Figure 6 shows synchrotron XRD patterns of the 2D PCP adsorbing various kinds of gases at several temperatures (methanol, ethanol, 1-propanol, and water at room temperature and CO_2 at 196 K). All of the XRD patterns of the gas-adsorbing 2D PCP are different from that of the guest-free PCP. Furthermore, they are different from each other, indicating a characteristic structure transformation depending on the nature of the adsorbing guests. The measured XRD patterns were indexed to estimate the interlayer distances and the distortion of the 2D SG by the DICVOL software.[85] The obtained index parameters for all cases are reported in Table 3S (Supporting Information). The determined *d* values, corresponding to the interlayer distances, are intermediate between that of the as-synthesized state and the guest-free state (see Table 2): methanol, 6.54 Å; ethanol, 6.57 Å; 1-propanol, 6.68 Å; water, 6.53 Å. The *d* values show that the free volume is moderately increased with respect to the guest-free species (6.30 Å). The square windows are less distorted, and in particular, ethanol and water adsorbing crystals show similar *a* and *b* unit cell parameters, typical of the open form (Figure 2b and Table 3S, Supporting Information).

The adsorption isotherms of N_2, CO_2, and Ar have the stepwise structure, as mentioned above. However, the adsorption isotherms of methanol, ethanol, and 1-propanol at 303 K on the 2D PCP have no definite folding points and/or adsorption jumps (Figure 8S, Supporting Information). Only the water adsorption isotherm has a gradual uptake around $P/P_0 = 0.07$, which must be caused by the weak hydrophobic nature of the framework. The rise of the isotherms in the low-pressure region depends on the hydrophobic tendency of adsorbate so that 1-propanol shows the steepest uptake in these adsorbates. The maximum adsorption molecular numbers of methanol, ethanol, 1-propanol, and water correspond to 4.1, 2.1, 0.94, and 4.8 per one Cu, respectively. On the other hand, the ratio of volumes of each molecules is almost 2.6:4.0:5.0:1. Therefore, the ratio of the occupied space in the micropores is 11:8.4:4.7:4.8 in the order of methanol, ethanol, 1-propanol, and water. In alcoholic adsorptions, the larger the molecular size of the adsorbate, the lower the density of the adsorbed phase, because of molecular packing difficulty in micropores. The adsorbed state of water is unique. In spite of the smaller molecular size of water when compared with that of the alcohol molecules, the adsorbed density is low. This must stem from the bulky hydrogen bonding network formed in the micropores.

The 2D PCP can form a variety of structural states at different pressures even with one kind of gas species. The synchrotron XRD patterns through the CO_2 adsorption at 196 K on the 2D PCP are shown in Figure 6b. The XRD patterns clearly show the structural changes occurring in sequence accompanied with CO_2 accommodation. The functions of flexible PCPs can be controlled not only by the type of gas species but also by the introduced gas pressure.

4. CONCLUSIONS

We established the selective synthetic way to flexible 2D/3D porous coordination polymers having a similar local coordination structure around the Cu(II) ions and exactly the same framework composition, $[Cu(bpy)_2(OTf)_2]_n$, in different solvent−solution systems. These species have proven to be useful for the investigation of the phenomenon of framework dimesionality-dependent gas adsorption. Although both kinds of PCPs have framework flexibility, the 2D PCP shows higher flexibility than that of the 3D PCP. The difference of the framework flexibility generates the different gas adsorption isotherms. The 3D PCP shows type I adsorption isotherms without definite steps. However, the 3D PCP shows the selective adsorption by the molecular sieving effect and quadrupole−hydrophilic surface interaction. On the other hand, the highly flexible 2D PCP shows stepwise adsorption isotherms for a variety of gases such as N_2, CO_2, Ar, CH_4, and water, by a concerted phenomenon involving the expansion/shrinkage of the layers and the breathing transformation. In particular, the uptakes of CO_2 and Ar on the 2D PCP are twice that on the 3D PCP, although the pore volume of the guest-free 2D PCP is less than one-half that of the 3D PCP. In alcohol adsorption isotherms, although the definite folding point is not observed, the 2D PCP changes its framework structure through the accommodation of guest molecules. Gas-adsorbing structures of the 2D PCP depend on the type of guest molecules and can be changed by variation of pressure. Hence, the 2D structure is indispensable to show a remarkable structure adaptability to molecular adsorption. The concept of using the expandable layered PCP must improve the functionalities such as molecular storage and separation.

■ ASSOCIATED CONTENT

Supporting Information. Crystallographic structures and parameters, IR spectra, adsorption isotherms, and microporous parameters. This material is available free of charge via the Internet at http://pubs.acs.org.

■ AUTHOR INFORMATION

Corresponding Author

kondoa@cc.tuat.ac.jp; kajiro.hiroshi@nsc.co.jp; kanoh@pchem2.s.chiba-u.ac.jp

Present Addresses

□Department of Applied Chemistry, Tokyo University of Agriculture and Technology, 2-24-16 Koganei, Naka-cho 184−8588, Japan.

■ ACKNOWLEDGMENT

The synchrotron radiation experiments were performed at SPring-8 with the approval of [Japan Synchrotron Radiation Research Institute (JASRI)] as Nanotechnology Support Project of the Ministry of Education, Culture, Sports, Science and Technology (Proposal No. 2006A1587/BL02B2). This work was supported in part by Japan Regional Innovation Strategy Program by the Excellence, JST, Global Center-of-Excellence program at Chiba University (G03, Advanced School for Organic Electronics) (MEXT), a Grant-in-Aid for Fundamental Scientific Research (B) (No. 19350100), and "Innovation Creative Center for Advanced Interdisciplinary Research Areas at Shinshu University" Project in Special Coordination Funds for Promoting Science and Technology of the Ministry of Education, Culture, Sports, Science and Technology, the Japanese Government.

REFERENCES

(1) Hoskins, B. F.; Robson, R. *J. Am. Chem. Soc.* **1990**, *112*, 1546–1554.
(2) Batten, S. R.; Robson, R. *Angew. Chem., Int. Ed.* **1998**, *37*, 1460–1494.
(3) Hagrman, D.; Hagrman, P. J.; Zubieta, J. *Angew. Chem., Int. Ed.* **1999**, *38*, 2638–2684.
(4) Moulton, B.; Zawarotko, M. J. *Chem. Rev.* **2001**, *101*, 1629–1658.
(5) Carlucci, L.; Ciani, G.; Proserpio, D. M. *Coord. Chem. Rev.* **2003**, *246*, 247–289.
(6) Carlucci, L.; Ciani, G.; Proserpio, D. M. *CrystEngCommun.* **2003**, *5*, 269–279.
(7) Kitagawa, S.; Kitaura, R.; Noro, S. *Angew. Chem., Int. Ed.* **2004**, *43*, 2334–2375.
(8) Kitagawa, S.; Matsuda, R. *Coord. Chem. Rev.* **2007**, *251*, 2490–2509.
(9) Baburin, I. A.; Blatov, V. A.; Carlucci, L.; Ciani, G.; Proserpio, D. M. *Cryst. Growth Des.* **2008**, *8*, 519–539.
(10) Li, H.; Eddaoudi, M.; O'Keeffe, M.; Yaghi, O. M. *Nature* **1999**, *402*, 276–279.
(11) Kondo, M.; Okubo, T.; Asami, A.; Noro, S.; Yoshitomi, T.; Kitagawa, S.; Ishii, T.; Matsuzaka, H.; Seki, K. *Angew. Chem., Int. Ed.* **1999**, *38*, 140–143.
(12) Li, D.; Kaneko, K. *J. Phys. Chem. B* **2000**, *104*, 8940–8945.
(13) Rowsell, J. L. C.; Yaghi, O. M. *Microporous Mesoporous Mater.* **2004**, *73*, 3–14.
(14) Seayad, A. M.; Antonelli, D. M. *Adv. Mater.* **2004**, *16*, 765–777.
(15) Panella, B.; Hirscher, M.; Pütter, H.; Müller, U. *Adv. Funct. Mater.* **2006**, *16*, 520–524.
(16) Collins, D. J.; Zhou, H.-C. *J. Mater. Chem.* **2007**, *17*, 3154–3160.
(17) Snurr, R. Q.; Hupp, J. T.; Nguyen, S. T. *AIChE J.* **2004**, *50*, 1090–1095.
(18) Choi, E.-Y.; Park, K.; Yang, C.-M.; Kim, H.; Son, J.-H.; Lee, S. W.; Lee, Y. H.; Min, D.; Kwon, Y.-U. *Chem.—Eur. J.* **2004**, *10*, 5535–5540.
(19) Maji, T. K.; Uemura, K.; Chang, H.-C.; Matsuda, R.; Kitagawa, S. *Angew. Chem., Int. Ed.* **2004**, *43*, 3269–3272.
(20) Dincă, M.; Long, J. R. *J. Am. Chem. Soc.* **2005**, *127*, 9376–9377.
(21) Maji, T. K.; Matsuda, R.; Kitagawa, S. *Nat. Mater.* **2007**, *6*, 142–148.
(22) Noguchi, D.; Tanaka, H.; Kondo, A.; Kajiro, H.; Noguchi, H.; Ohba, T.; Kanoh, H.; Kaneko, K. *J. Am. Chem. Soc.* **2008**, *130*, 6367–6372.
(23) Seo, J. S.; Wand, D.; Lee, H; Jun, S. I.; Oh, J.; Jeon, Y.; Kim, K. *Nature* **2000**, *404*, 982–986.
(24) Moon, H. R.; Kim, J. H.; Suh, M. P. *Angew. Chem., Int. Ed.* **2005**, *44*, 1261–1265.
(25) Wu., C.-D.; Hu, A.; Zhang, L.; Lin, W. *J. Am. Chem. Soc.* **2005**, *127*, 8940–8941.
(26) Arai, T.; Takasugi, H.; Sato, T.; Noguchi, H.; Kanoh, H.; Kaneko, K.; Yanagisawa, A. *Chem. Lett.* **2005**, *34*, 1590–1591.
(27) Wu., C.-D.; Lin, W. *Angew. Chem., Int. Ed.* **2007**, *46*, 1075–1078.
(28) Ma, L.; Abney, C.; Lin, W. *Chem. Soc. Rev.* **2009**, *38*, 1248–1256.
(29) Haldler, G. J.; Kepert, C. J.; Moubaraki, B.; Murray, K. S.; Cashion, J. D. *Science* **2002**, *298*, 1762–1765.
(30) Real, J. A.; Andrés, E.; Muñoz, M. C.; Julve, M.; Granier, T.; Bousseksou, A.; Varret, F. *Science* **1995**, *268*, 265–267.
(31) Maspoch, D.; Ruizmolina, D.; Wurst, K.; Domingo, N.; Cavallini, M.; Biscarini, F.; Tejada, J.; Rovira, C.; Veciana, J. *Nat. Mater.* **2003**, *2*, 190–195.
(32) Maspoch, D.; Ruiz-Molina, D.; Veciana, J. *J. Mater. Chem.* **2004**, 2713–2723.
(33) Navarro, J. A. R.; Barea, E.; Rodriguez-Dieguez, A.; Salas, J. M.; Ania, C. O.; Parra, J. B.; Masciocchi, N.; Galli, S.; Sironi, A. *J. Am. Chem. Soc.* **2008**, *130*, 3978–3984.
(34) Kurmoo, M. *Chem. Soc. Rev.* **2009**, *38*, 1353–1379.
(35) Katz, H. E.; Scheller, G.; Putvinski, T. M.; Schilling, M. L.; Wilson, W. L.; Chidsey, C. E. D. *Science* **1991**, *254*, 1485–1487.
(36) Lin, W.; Lin, W.; Wong, G. K.; Marks, T. J. *J. Am. Chem. Soc.* **1996**, *118*, 8034–8042.
(37) Evans, O. R.; Lin, W. *Acc. Chem. Res.* **2002**, *35*, 511–522.
(38) Janiak, C. *Dalton Trans.* **2003**, *14*, 2781–2804.
(39) Min, K. S.; Suh, M. P. *J. Am. Chem. Soc.* **2000**, *122*, 6834–6840.
(40) Biradha, K.; Fujita, M. *Angew. Chem., Int. Ed.* **2002**, *41*, 3392–3395.
(41) Takamizawa, S.; Nakata, E.; Yokoyama, H.; Mochizuki, K.; Mori, W. *Angew. Chem., Int. Ed.* **2003**, *42*, 4331–4334.
(42) Rosseinsky., M. J. *Microporous Mesoporous Mater.* **2004**, *73*, 15–30.
(43) Dybtsev, D. N.; Chun, H.; Kim., K. *Angew. Chem., Int. Ed.* **2004**, *43*, 5033–5036.
(44) Sudik, A. C.; Millward, A. R.; Ockwig, N. W.; Côté, A. P.; Kim, J.; Yaghi, O. M. *J. Am. Chem. Soc.* **2005**, *127*, 7110–7118.
(45) Halder, G. J.; Kepert, C. J. *J. Am. Chem. Soc.* **2005**, *127*, 7891–7900.
(46) Suh, M. P.; Moon, H. R.; Lee, E. Y.; Jang, S. Y. *J. Am. Chem. Soc.* **2006**, *128*, 4710–4718.
(47) Serre, C.; Bourrelly, S.; Vimont, A.; Ramsahye, N. A.; Maurin, G.; Llewellyn, P. L.; Daturi, M.; Filinchuk, Y.; Leynaud, O.; Barnes, P.; Férey, G. *Adv. Mater.* **2007**, *19*, 2246–2251.
(48) Uemura, K.; Yamasaki, Y.; Komagawa, Y.; Tanaka, K.; Kita, H. *Angew. Chem., Int. Ed.* **2007**, *46*, 6662–6665.
(49) Shimomura, S.; Horike, S.; Matsuda, R.; Kitagawa, S. *J. Am. Chem. Soc.* **2007**, *129*, 10990–10991.
(50) Bradshaw, D.; Warren, J. E.; Rosseinsky, M. J. *Science* **2007**, *315*, 977–980.
(51) Ma, S.; Sun, D.; Simmons, J. M.; Collier, C. D.; Yuan, D.; Zhou, H.-C. *J. Am. Chem. Soc.* **2008**, *130*, 1012–1016.
(52) Choi, H. J.; Dincă, M.; Long, J. R. *J. Am. Chem. Soc.* **2008**, *130*, 7848–7850.
(53) Culp, J. T.; Smith, M. R.; Bittner, E.; Bockrath, B. *J. Am. Chem. Soc.* **2008**, *130*, 12427–12434.
(54) Tanaka, D.; Kitagawa, S. *Chem. Mater.* **2008**, *20*, 922–931.
(55) Férey, G. *Chem. Soc. Rev.* **2008**, *37*, 191–214.
(56) Horike, S.; Shimomura, S.; Kitagawa, S. *Nature Chem.* **2009**, *1*, 695–704.
(57) Kondo, A.; Chinen, A.; Kajiro, H.; Nakagawa, T.; Kato, K.; Takata, M.; Hattori, Y.; Okino, F.; Ohba, T.; Kaneko, K.; Kanoh, H. *Chem.—Eur. J.* **2009**, *31*, 7549–7553.
(58) Kondo, A.; Nakagawa, T.; Kajiro, H.; Chinen, A.; Hattori, Y.; Okino, F.; Ohba, T.; Kaneko, K.; Kanoh, H. *Inorg. Chem.* **2010**, *49*, 9247–9252.
(59) Kajiro, H.; Kondo, A.; Kaneko, K.; Kanoh, H. *Int. J. Mol. Sci.* **2010**, *11*, 3803–3845.
(60) Kitagawa, S.; Matsuda, R. *Coord. Chem. Rev.* **2007**, *251*, 2490–2509.
(61) Noro, S.; Tanaka, D.; Sakamoto, H.; Shimomura, S.; Kitagawa, S.; Takeda, S.; Uemura, K.; Kita, H.; Akutagawa, T.; Nakamura, T. *Chem. Mater.* **2009**, *21*, 3344–3355.
(62) Li, D.; Kaneko, K. *Chem. Phys. Lett.* **2001**, *335*, 50–56.
(63) Noguchi, H.; Kondo, A.; Hattori, Y.; Kajiro, H.; Kanoh, H.; Kaneko, K. *J. Phys. Chem. C* **2007**, *111*, 248–254.
(64) Kanoh, H.; Kondo, A.; Noguchi, H.; Kajiro, H.; Tohdoh, A.; Hattori, Y.; Xu, W.-C.; Inoue, M.; Sugiura, T.; Morita, K.; Tanaka, H.; Ohba, T.; Kaneko, K. *J. Colloid Interface Sci.* **2009**, *334*, 1–7.
(65) Kondo, A.; Noguchi, H; Ohnishi, S.; Kajiro, H.; Tohdoh, A.; Hattori, Y.; Xu, W.-C.; Tanaka, H.; Kanoh, H.; Kaneko, K. *Nano Lett.* **2006**, *6*, 2581–2584.
(66) Noguchi, H.; Kondo, A.; Hattori, Y.; Kanoh, H.; Kajiro, H.; Kaneko, K. *J. Phys. Chem. B* **2005**, *109*, 13851–13853.
(67) Kondo, A.; Noguchi, N.; Carlucci, L.; Proserpio, D. M.; Ciani, G.; Kajiro, H.; Kanoh, H.; Kaneko, K. *J. Am. Chem. Soc.* **2007**, *129*, 12362–12363.

(68) Serre, C.; Millange, F.; Thouvenot, C.; Noguès, M.; Marsolier, G.; Louër, D.; Férey, G. *J. Am. Chem. Soc.* **2002**, *124*, 13519–13526.
(69) Bourrelly, S.; Llewellyn, P. L.; Serre, C.; Millange, F.; Loiseau, T.; Férey, G. *J. Am. Chem. Soc.* **2005**, *127*, 13519–13521.
(70) Sluis, P. v. d.; Speck, A. L. *Acta Crystallogr., Sect. A* **1990**, *46*, 194.
(71) Crystal data for **3**: Several data collections were performed at 150 K for compound **3**. We were able to solve and locate the atoms, but due to the low quality of the data it is not possible to provide a final cif file. It is isomorphous with **4** and strictly related to **1** and **2**. The unit cell and the extracted layer parameters are, in any case, significant and useful for comparison with the other 2D structures (**1**, **2**, **4**). Crystal data for **4**: 18 472 reflections measured, 4143 unique (R_{int} = 0.0558) used in all calculations. The final agreement index R_1 was 0.0704 (0.1091 before SQUEEZE) for 2501 independent significant [$I > 2\sigma(I)$] absorption corrected data and 208 parameters and 24 restraints, [$wR(F^2)$ = 0.2133 for all data], GOF = 1.072. Crystal data for **5**: 80 617 reflections measured, 4416 unique (R_{int} = 0.0720) used in all calculations. The final agreement index R_1 was 0.0871 (0.1151 before SQUEEZE) for 3552 independent significant [$I > 2\sigma(I)$] absorption corrected data and 186 parameters and 6 restraints [$wR(F_2)$ = 0.2542 for all data], GOF = 1.063. Crystal data for **6**: 79 208 reflections measured, 4144 unique (R_{int} = 0.0413) used in all calculations. The final agreement index R_1 was 0.0899 (0.1236 before SQUEEZE) for 3674 independent significant [$I > 2\sigma(I)$] absorption corrected data and 186 parameters and 6 restraints, [$wR(F_2)$ = 0.2636 for all data], GOF = 1.044.Crystal data for **7**: 38 911 reflections measured, 4455 unique (R_{int} = 0.0819) used in all calculations. The final agreement index R_1 was 0.0992 (0.1599 before SQUEEZE) for 3091 independent significant [$I > 2\sigma(I)$] absorption corrected data and 186 parameters and 6 restraints, [$wR(F_2)$ = 0.2754 for all data], GOF = 1.081.
(72) Nishibori, E.; Takata, M.; Kato, K.; Sakata, M.; Kubota, Y.; Aoyagi, S.; Kuroiwa, Y.; Yamakata, M.; Ikeda, N. *Nucl. Instrum. Methods A* **2001**, *467−468*, 1045–1048.
(73) Spek, A. L. *PLATON, A Multipurpose Crystallographic Tool*; Utrecht University: Utrecht, The Netherlands, 1999.
(74) Carlucci, L.; Cozzi, N.; Ciani, G.; Moret, M.; Proserpio, D. M.; Rizzato, S. *Chem. Commun.* **2002**, 1354–1355.
(75) Bering, B. P.; Dubinin, M. M.; Serpinsky, V. V. *J. Colloid Interface Sci.* **1966**, *21*, 378–393.
(76) Bojan, M. J.; Steele, W. A. *Carbon* **1998**, *36*, 1417–1423.
(77) Murthy, C. S.; Singer, K.; Klein, M. L.; McDonald, I. R. *Mol. Phys.* **1980**, *41*, 1387–1399.
(78) Gregg, S. J.: Sing, K. S. W. *Adsorption, Surface Area and Porosity*; Academic Press: London, 1982.
(79) Miles, M. G.; Doyle, G.; Cooney, R. P.; Tobias, R. S. *Spectrochim. Acta* **1969**, *25A*, 1515–1526.
(80) Nicholson, D.; Gubbins, K. E. *J. Chem. Phys.* **1996**, *104*, 8126–8134.
(81) Seki, K.; Kitagawa, S. *Chem. Phys. Phys. Chem.* **2002**, *4*, 1968–1971.
(82) Zhao, X.; Xiao, B.; Fletcher, A. J.; Thomas, K. M.; Bradshaw, D.; Rosseinsky, M. J. *Science* **2004**, *306*, 1012–1015.
(83) Choi, H. J.; Dincă, M.; Long, J. R. *J. Am. Chem. Soc.* **2008**, *130*, 7848–7850.
(84) Kaneko, K. *Colloids Surf.* **1989**, *37*, 115–124.
(85) Boultif, A.; Loüer, D. *J. Appl. Phys.* **1991**, *24*, 987–993.